12 Apr 2016

Big Changes for Small Noncovalent Dimers: Revisiting the Potential Energy Surfaces of (P2)2 and (Pccp)2 with Ccsd(T) Optimizations and Vibrational Frequencies

Eric Van Dornshuld

Gregory S. Tschumper
Missouri University of Science and Technology, gtschumper@mst.edu

Recommended Citation

E. Van Dornshuld and G. S. Tschumper, "Big Changes for Small Noncovalent Dimers: Revisiting the Potential Energy Surfaces of (P2)2 and (Pccp)2 with Ccsd(T) Optimizations and Vibrational Frequencies," *Journal of Chemical Theory and Computation*, vol. 12, no. 4, pp. 1534 - 1541, American Chemical Society, Apr 2016.
The definitive version is available at https://doi.org/10.1021/acs.jctc.5b01105

JCTC Journal of Chemical Theory and Computation

Article

pubs.acs.org/JCTC

Big Changes for Small Noncovalent Dimers: Revisiting the Potential Energy Surfaces of $(P_2)_2$ and $(PCCP)_2$ with CCSD(T) Optimizations and Vibrational Frequencies

Eric Van Dornshuld[†] and Gregory S. Tschumper*

Department of Chemistry and Biochemistry, University of Mississippi, University, Mississippi 38677-1848, United States

Supporting Information

ABSTRACT: This article details the re-examination of low-lying stationary points on the potential energy surfaces (PESs) of two challenging noncovalent homogeneous dimers, $(P_2)_2$ and $(PCCP)_2$. The work was motivated by the rather large differences between MP2 and CCSD(T) energetics that were recently reported for these systems (*J. Comput. Chem.* **2014**, *35*, 479−487). The current investigation reveals significant qualitative and quantitative changes when the CCSD(T) method is used to characterize the stationary points instead of MP2. For example, CCSD(T) optimizations and harmonic vibrational frequency computations with the aug-cc-pVTZ basis set indicate that the parallel-slipped (PS) structure is the only P_2 dimer stationary point examined that is a minimum (zero imaginary frequencies, $n_i = 0$), whereas prior MP2 computations indicated that it was a transition state ($n_i = 1$). Furthermore, the L-shaped structure of $(P_2)_2$ was the only minimum according to MP2 computations, but it collapses to the PS structure on the CCSD(T)/aug-cc-pVTZ PES. For the larger PCCP dimer, the CCSD(T) computations reveal that four rather than just two of the six stationary points characterized are minima. A series of explicitly correlated single-point energies were computed for all of the optimized structures to estimate the MP2 and CCSD(T) electronic energies at the complete basis set limit. CCSDT(Q) computations were also performed to assess the effects of dynamical electron correlation beyond the CCSD(T) level. For both $(P_2)_2$ and $(PCCP)_2$, dispersion remains the dominant attractive component to the interaction energy according to symmetry-adapted perturbation theory analyses, and it is also the most challenging component to accurately evaluate.

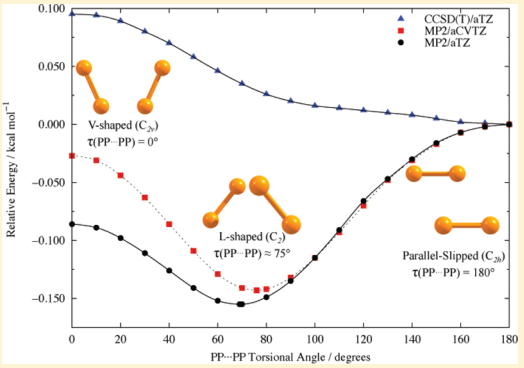

1. INTRODUCTION

Noncovalent interactions play important roles in chemical and biological processes.[1−6] However, these interactions can require computationally prohibitive quantum mechanical methods to accurately quantify them. Despite their small size, the dispersion-bound homogeneous dimers of P_2 and PCCP [i.e., $(P_2)_2$ and $(PCCP)_2$] exemplify this challenge.[7−9] It was shown, for example, that second-order Møller−Plesset perturbation theory (MP2)[10] overbinds the PCCP dimer by as much as 3.2 kcal mol^{-1} relative to that with CCSD(T)[11,12] (i.e., the coupled-cluster method that includes all single and double substitutions as well as a perturbative treatment of the connected triple excitations) interaction energies at the complete basis set (CBS) limit.[8] This overbinding increased to as much as 5 kcal mol^{-1} when the geometries were fully optimized with the MP2 method,[9] which is remarkable considering that the CCSD(T) CBS limit binding energy is only about −1.2 kcal mol^{-1}. These differences are far more pronounced than those for other small dispersion bound dimers such as the N_2 dimer[13] and the acetylene dimer.[14] For noncovalent complexes containing first-row atoms, the deviation between MP2 and CCSD(T) interaction/binding energies increases when both fragments contain delocalized π-electron clouds, starting off near 1.0 kcal mol^{-1} in the diacetylene dimer[15−17] and the cyanogen dimer[15] and growing as large as 2.0 kcal mol^{-1} in face-to-face configurations of the benzene dimer.[18] It is worth noting that MP2 was shown to overbind the P_2 dimer by as much as 1.5 kcal mol^{-1} at the CBS limit relative to that with CCSD(T) even though there is no delocalized π-electron system.[9]

The relatively diminutive size of P_2 and PCCP facilitates a thorough and rigorous characterization of the stationary points on the corresponding dimer potential energy surfaces (PESs) with coupled-cluster theory. Previous work has characterized various configurations of the P_2 and PCCP dimers on the MP2 PES. It was shown that reliable optimized structures could be obtained with a triple-ζ basis set for these dimers.[9] However, the aforementioned large discrepancies between MP2 and CCSD(T) energetics for these two systems led to some inconsistencies regarding the nature and ordering of some stationary points. These results suggested that a consistent description of both noncovalent dimers would likely require

Received: November 19, 2015
Published: March 21, 2016

DOI: 10.1021/acs.jctc.5b01105
J. Chem. Theory Comput. 2016, 12, 1534−1541

characterization of all stationary points with the CCSD(T) method and a basis set of aug-cc-pVTZ quality.

This article presents the first investigation implementing the CCSD(T) method to characterize a variety of stationary points on the PESs of the challenging $(P_2)_2$ and $(PCCP)_2$ noncovalent dimers. Explicitly correlated methods are used in conjunction with large correlation consistent basis sets to estimate the CBS limit energetics of these optimized stationary points. Although electron correlation effects beyond the CCSD(T) level have been found to be quite small in other weakly bound dimers,[19−26] they could be more significant here given the large differences among MP2, CCSD, and CCSD(T) energies.[8] As such, CCSDT(Q) computations (where a perturbative treatment of the connected quadruple excitations are added to an iterative CCSDT computation)[27] are also carried out for each stationary point with a basis set of at least aug-cc-pVDZ quality following the recommendations of Smith et al.[26] In addition, the performance of other methods is examined, such as dispersion-corrected density functional theory, spin-component-scaled MP2 (SCS-MP2), scaled MP3 (MP2.5), coupled MP2 (MP2C), and spin-component-scaled CCSD (SCS-CCSD), including the variant with scaling parameters optimized for molecular interactions (SCS(MI)-CCSD). Finally, the components to the interaction energy are probed with wave-function-based symmetry-adapted perturbation theory (SAPT) for all dimer structures.

2. THEORETICAL METHODS

Full geometry optimizations and corresponding harmonic vibrational frequency computations were carried out using the CCSD(T) electronic structure method for each geometry. The aug-cc-pVTZ (aTZ) basis set[28,29] was employed for these computations because our previous investigation revealed that the triple- and quadruple-ζ correlation consistent basis sets gave very similar results for these complexes with the MP2 method.[9] These CCSD(T) computations were performed with the CFOUR[30] software package using the available analytic gradients and Hessians. Binding energies, E_{bind}, for the dimers were determined via the supermolecular approach by comparing the energy of each optimized dimer configuration to the corresponding energies of the optimized monomers. In contrast, interaction energies (E_{int}) were calculated using monomer energies computed at the geometries that they adopt in each dimer structure (i.e., without monomer relaxation/distortion effects).

Single-point energies were computed for each CCSD(T)/aTZ-optimized structure with explicitly correlated MP2 and CCSD(T) methods (specifically, MP2-F12 3C(FIX) and CCSD(T)-F12b with unscaled triples contributions, respectively) in conjunction with the a5Z basis set. This protocol was shown to yield nearly identical energetics for these dimers as those obtained with popular CBS extrapolation techniques for canonical MP2 and CCSD(T) correlation energies.[9] These computations, including the spin-component-scaled MP2 variant (SCS-MP2-F12),[31] were conducted with the Molpro2010.1[32] program employing the default density fitting (DF) and resolution of the identity (RI) basis sets. For the SCC-MP2-F12 computations, the singlet and triplet scaling factors were 6/5 and 1/3,[31] respectively, for the SCS parameters. CCSDT(Q) electronic energies were also computed with the aug-cc-pVDZ (aDZ) basis using a developmental version of the CFOUR software package.[30] To gauge the effect of the inconsistency commonly referred basis set superposition error[33] near the estimated CBS limit, the counterpoise (CP) procedure[34,35] was also applied to the CCSD(T)-F12/a5Z computations following the procedures outlined in detail elsewhere.[36]

Wave-function-based SAPT analyses were performed for all CCSD(T)/aTZ-optimized structures to gain insight into the interactions of each dimer's geometry. The contributions from dispersion (E_{disp}), electrostatics (E_{elec}), induction (E_{ind}), and exchange repulsion (E_{exch}) to the total interaction energy (E_{int}) were computed with the SAPT2, SAPT2+, SAPT2+3, and SAPT2+3(CCD) methods[7,37] along with the aTZ basis set. These computations employed the default DF and RI basis sets in the PSI4 software package.[38]

Four dispersion-corrected density functional methods were also used to characterize the $(P_2)_2$ and $(PCCP)_2$ systems: B97-D3BJ,[39,40] B3LYP-D3BJ,[40−42] ωB97X-D,[43] and APFD.[44] All density functional theory (DFT) computations (single-point energies, geometry optimizations, and harmonic vibrational frequencies) were performed in Gaussian 09[45] with a pruned numerical integration grid having 150 radial shells and 974 angular points per shell.

A variety of other methods were also used in conjunction with the aTZ basis set to compute interaction energies. These include two spin-component-scaled CCSD procedures (SCS-CCSD[46] and SCS(MI)-CCSD[47]), a scaled MP3[48,49] technique (MP2.5[50]), and the coupled MP2 method (MP2C[51,52]). The MP2C computations followed the prescription of Heßelmann except that neither the frozen-core approximation nor density fitting was employed to evaluate the correction to the MP2 interaction energy (ΔMP2C). This minor alteration of the procedure introduced only small changes relative to the ΔMP2C values reported elsewhere (e.g., <0.05 kcal mol^{-1} for the benzene···HCN complex).[52] PSI4 and Molpro2010.1 were used to perform these single-point energy computations.

Spherical harmonic basis functions (5d, 7f, etc.) were used for all computations. Residual Cartesian gradients of optimized structures were less than 10^{-7} $E_h a_0^{-1}$. The frozen-core approximation was invoked for all post-Hartree−Fock computations (1s-, 2s-, and 2p-like orbitals on phosphorus, and 1s-like orbitals on carbon), with the aforementioned exception of the ΔMP2C correction.

3. RESULTS AND DISCUSSION

3.1. P_2 Dimer Stationary Points. Our previous study identified eight $(P_2)_2$ stationary points on the MP2 PES with a variety of triple- and quadruple-ζ correlation consistent basis sets. The configurations are shown in Figure 1 and include the parallel-slipped structure (PS) with C_{2h} symmetry, the rectangle structure (Rec) with D_{2h} symmetry, the perpendicular X-shaped structure ($\perp$X) with D_{2d} symmetry, the V-shaped structure (V) with C_{2v} symmetry, the nonplanar T structure (npT) with C_s symmetry, the L-shaped structure (L) with C_2 symmetry, the T-shaped structure (T) with C_{2v} symmetry, and the linear structure (Lin) with $D_{\infty h}$ symmetry. The MP2-optimized structures served as the starting point for the CCSD(T) geometry optimizations with the aTZ basis set. All stationary points were readily located on the CCSD(T)/aTZ PES except the L-shaped structure that collapses to the PS configuration. Scans about the PP···PP torsional angle from 0° (corresponding to the V-shaped structure) to 180° (corresponding to the PS configuration) confirm the absence of this C_2 stationary point on the CCSD(T)/aTZ PES. (See the Supporting Information.)

DOI: 10.1021/acs.jctc.5b01105
J. Chem. Theory Comput. 2016, 12, 1534−1541

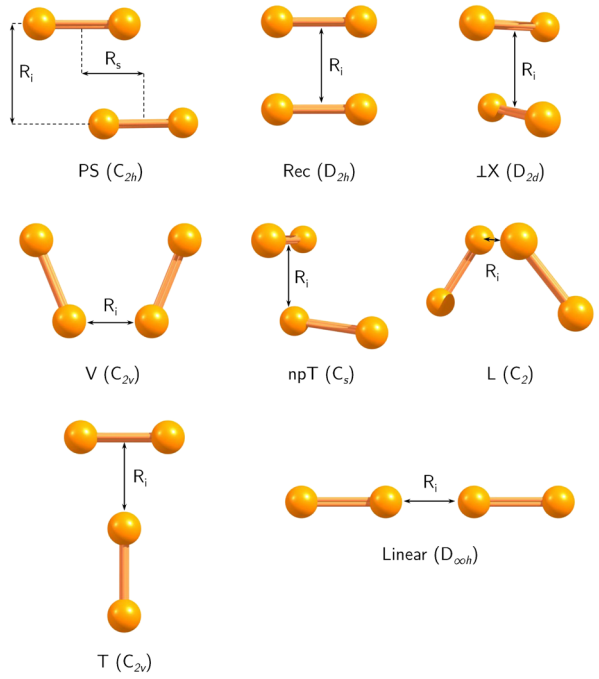

Figure 1. P_2 dimer structures and select intermolecular parameters. Note that the L-shaped structure collapses to the PS stationary point when it is optimized at the CCSD(T)/aTZ level of theory.

Select intermolecular separations (R_i and R_s, shown in Figure 1) and the number of imaginary frequencies (n_i) from the CCSD(T)/aTZ computations are listed in Table 1 for each stationary point. The intermolecular bond angle, θ, defined as the angle between a terminal P atom and the R_i intermolecular axis, is also reported for V and npT configurations. The corresponding MP2/aCVQZ results from ref 9 are also provide for comparison. We note that both basis set and core correlation effects on the geometry were small between the frozen-core MP2/aTZ and all-electron MP2/aCVQZ computations, where R_i and R_s differed by less than 0.1 Å and θ differed by less than 3°.[9]

The CCSD(T)/aTZ characteristics of the P_2 monomer (Supporting Information) are very similar to previously reported MP2/aCVQZ results. The optimized PP bond lengths differ by roughly 0.01 Å, and the corresponding harmonic vibrational frequencies, by 31 cm^{-1}. The differences in the intermolecular geometrical parameters are far larger, however, due to the appreciable overbinding of the P_2 dimer at the MP2 level of theory. The optimized CCSD(T) R_i values in Table 1 are typically 0.3 to 0.4 Å longer than the corresponding MP2 values.

CCSD(T)/aTZ harmonic vibrational frequencies reveal significant qualitative changes in the nature of certain stationary points relative to the MP2/aCVQZ computations. As mentioned earlier, the L-shaped minimum on the MP2 surface does not appear to correspond to a stationary point at the CCSD(T)/aTZ level of theory. Instead, the PS structure is the only minimum on the CCSD(T) PES (n_i = 0), even though it was a transition state (n_i = 1) according to previous MP2 computations. The V structure changes from a transition state (n_i = 1) on the MP2 PES to a second-order saddle point (n_i = 2) according to CCSD(T)/aTZ computations. Although n_i did not change for the other stationary points, it is clear that the MP2 and CCSD(T) PESs for the small P_2 dimer are qualitatively quite different. The Cartesian coordinates and harmonic vibrational frequencies for all of the CCSD(T)/aTZ-optimized structures can be found in the Supporting Information.

3.2. PCCP Dimer Stationary Points. All six $(PCCP)_2$ stationary points previously characterized with MP2 computations have been located on the CCSD(T)/aTZ PES. The configurations are shown in Figure 2 and include the parallel-slipped structure (PS) with C_{2h} symmetry, the X-shaped structure (X) with D_2 symmetry, the perpendicular X-shaped structure (⊥X) with D_{2d} symmetry, the rectangle structure (Rec) with D_{2h} symmetry, the T-shaped structure (T) with C_{2v} symmetry, and the linear (Lin) structure with $D_{\infty h}$ symmetry.

Select intermolecular separations (R_i and R_s, shown in Figure 2) and the number of imaginary frequencies (n_i) from the CCSD(T)/aTZ computations are listed in Table 2 for each stationary point. The intermolecular torsional angle, τ, defined as the torsional angle between two the CC bonds about the R_i axis, is also reported for the X configuration. Note that τ = 90.0° for the ⊥X structure. Lastly, an estimate of the CCSD(T) CBS limit binding energy (E_{bind}) from CCSD(T)-F12/a5Z computations is provided for each optimized structure. The corresponding MP2/aCVQZ results from ref 9 are also provide for comparison. Again, a previous investigation demonstrated that both basis set and core correlation effects on the geometry were small between the frozen-core MP2/aTZ and all-electron MP2/aCVQZ computations, where R_i and R_s differed by less than 0.1 Å and τ differed by less than 2°.[9] In $(PCCP)_2$, the

Table 1. Select Intermolecular Parameters of the MP2/aCVQZ- and CCSD(T)/aTZ-Optimized $(P_2)_2$ Structures as Well as the Number of Imaginary Vibrational Frequencies and Corresponding CCSD(T)-F12/a5Z Electronic Binding Energies[a]

	MP2/aCVQZ [ref 9]				CCSD(T)/aTZ [this work]			
geometry	n_i	R_i	R_s/θ^b	$E_{bind}{}^c$	n_i	R_i	R_s/θ^b	$E_{bind}{}^d$
PS	1	3.62	2.31	−0.78	0	4.03	2.21	−1.01
npT	1	3.82	96.7	−0.71	1	4.14	102.4	−0.94
⊥X	**1**	3.96		−0.63	**1**	4.33		−0.90
V	1	3.56	112.1	−0.58	2	3.92	114.3	−0.89
Rec	3	4.15		−0.53	3	4.51		−0.76
T	3	4.05		−0.50	3	4.32		−0.63
Lin	**2**	3.56		−0.42	**2**	4.14		−0.51
L	0	3.51	105.7	−0.65				

[a]Intermolecular parameters R and θ are in Å and degrees, respectively. The number of imaginary vibrational frequencies is in bold for doubly-degenerate modes. Electronic binding energies (E_{bind}) are in kcal mol^{-1}. [b]R_s for PS. θ for V, L, and npT. [c]CCSD(T)-F12/a5Z energies are at MP2/aCVQZ-optimized geometries. [d]CCSD(T)-F12/a5Z energies are at CCSD(T)/aTZ-optimized geometries.

DOI: 10.1021/acs.jctc.5b01105
J. Chem. Theory Comput. 2016, 12, 1534−1541

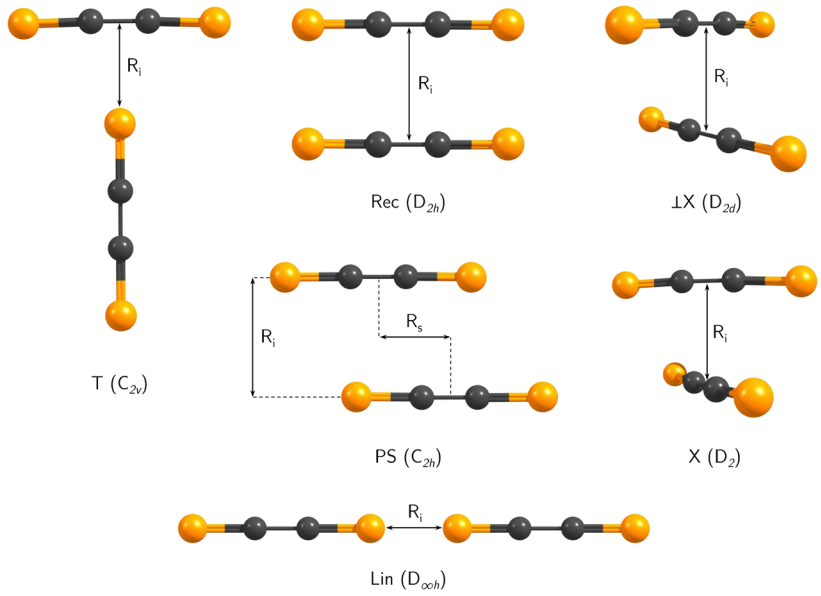

Figure 2. PCCP dimer structures and select intermolecular parameters.

Table 2. Select Intermolecular Parameters of the MP2/aCVQZ- and CCSD(T)/aTZ-Optimized $(PCCP)_2$ Structures as Well as the Number of Imaginary Vibrational Frequencies and Corresponding CCSD(T)-F12/a5Z Electronic Binding Energies[a]

	MP2/aCVQZ [ref 9]				CCSD(T)/aTZ [this work]			
geometry	n_i	R_i	R_s/τ[b]	E_{bind}[c]	n_i	R_i	R_s/τ[b]	E_{bind}[d]
PS	0	3.37	1.82	−2.17	0	3.76	1.82	−2.89
X	0	3.31	49.0	−1.20	0	3.51	80.2	−2.58
⊥X	1	3.20	90.0	−1.79	1	3.50	90.0	−2.57
Rec	2	3.79		−1.12	2	4.13		−1.88
T	2	3.39		−1.42	0	3.61		−1.74
Lin	**2**	3.84		−0.45	0	3.94		−0.56

[a]Intermolecular parameters R and τ are in Å and degrees, respectively. The number of imaginary vibrational frequencies is in bold for doubly-degenerate modes. Electronic binding energies (E_{bind}) are in kcal mol^{-1}. [b]R_s for PS. τ for X and ⊥X ($\tau \equiv 90°$ for D_{2d} ⊥X configuration). [c]CCSD(T)-F12/a5Z energies are at MP2/aCVQZ-optimized geometries. [d]CCSD(T)-F12/a5Z energies are at CCSD(T)/aTZ-optimized geometries.

individual fragments tend to be slightly bowed (nonlinear) in most of the MP2- and CCSD(T)-optimized structures. These slight distortions are also observed in the dimers of cyanogen[15] and diacetylene.[15,17]

As with P_2, the CCSD(T)/aTZ-optimized bond lengths and harmonic vibrational frequencies of the linear PCCP monomer (Supporting Information) are very similar to our previously reported MP2/aCVQZ results. The optimized bond lengths differ by roughly 0.01 Å, and the harmonic vibrational frequencies never deviate by more than 25 cm^{-1}. In contrast, the differences in the intermolecular geometrical parameters are far larger, however, due to the appreciable overbinding of the PCCP dimer at the MP2 level of theory. The optimized CCSD(T) R_i values in Table 2 are typically about 0.3 Å longer than the corresponding MP2 values.

The CCSD(T)/aTZ harmonic vibrational frequencies reveal only two modest qualitative changes in the nature of a stationary point. MP2 computations suggested the T and Lin configurations were second-order saddle points (n_i = 2), whereas they are minima (n_i = 0) at the CCSD(T)/aTZ level (Table 2). The magnitudes of the frequencies in question, however, are quite small (often <10 cm^{-1}), which suggests that the differences are not that severe. Along with the PS and X structures, this analysis yields a total of four minima on the CCSD(T)/aTZ surface compared to only two for MP2. The ⊥X stationary point is a transition state at both levels of theory, whereas the Rec structure is a higher-order saddle point. The Cartesian coordinates and harmonic vibrational frequencies for all of the CCSD(T)/aTZ-optimized structures can be found in the Supporting Information.

3.3. Energetics. *3.3.1. Binding Energies.* An estimate of the CCSD(T) CBS limit binding energy (E_{bind}) from CCSD(T)-F12/a5Z computations is provided for each optimized structure in Tables 1 and 2. For $(P_2)_2$, reoptimization at the CCSD(T)/aTZ level of theory increases the E_{bind} values by a few tenths of a kcal mol^{-1} (or roughly 30%) relative to those for the MP2/aCVQZ-optimized structures (fifth and last columns of Table 1). In the case of $(PCCP)_2$, the changes to E_{bind} tend to be even more pronounced. Reoptimizing the MP2/aCVQZ structures with the CCSD(T) method and aTZ basis set increases E_{bind} by more than 0.7 kcal mol^{-1} for the PS, ⊥X, and Rec configurations, whereas E_{bind} increases by nearly 1.4 kcal mol^{-1} for the X structure (fifth and last columns of Table 2).

The counterpoise procedure was also employed to determine the CCSD(T)-F12 binding energies of each optimized structure with the a5Z basis set. These E_{bind}^{CP} values are tabulated in the Supporting Information and deviate by no more than 0.02 kcal mol^{-1} from the corresponding data in Tables 1 and 2. An independent estimate of E_{bind} at the CCSD(T) CBS limit was also generated by extrapolating the

DOI: 10.1021/acs.jctc.5b01105
J. Chem. Theory Comput. 2016, 12, 1534−1541

Table 3. CCSDT(Q) Binding Energies and Differences Associated with the Corresponding CCSD(T) Values ($\delta^{CCSDT(Q)}_{CCSD(T)}$ in Parentheses)[a]

	P_2 dimer				PCCP dimer		
	aDZ[b]	aTZ[b]	aDZ[c]	aTZ[c]		aDZ[b]	aDZ[c]
PS	−0.697	−0.777	−0.996	−1.035	PS	−2.289	−3.023
	(−0.011)	(+0.016)	(+0.000)	(+0.019)		(+0.027)	(+0.034)
npT	−0.628	−0.726	−0.935	−0.976	X	−2.280	−2.830
	(−0.013)	(+0.016)	(−0.001)	(+0.020)		(+0.028)	(+0.045)
⊥X	−0.554	−0.676	−0.853	−0.934	⊥X	−1.429	−2.826
	(−0.017)	(+0.013)	(−0.002)	(+0.019)		(−0.043)	(+0.044)
V	−0.649	−0.645	−1.003	−0.946	Rec	−1.413	−1.991
	(−0.024)	(+0.002)	(−0.005)	(+0.013)		(−0.086)	(−0.010)
Rec	−0.587	−0.613	−0.770	−0.817	T	−1.839	−2.106
	(−0.026)	(−0.003)	(−0.006)	(+0.010)		(+0.007)	(+0.015)
T	−0.717	−0.649	−0.791	−0.738	Lin	−1.097	−1.088
	(−0.012)	(+0.001)	(−0.003)	(+0.008)		(−0.015)	(−0.002)
Lin	−0.801	−0.694	−0.803	−0.702			
	(−0.009)	(−0.004)	(−0.002)	(+0.002)			
L	−0.588	−0.665					
	(−0.018)	(+0.011)					

[a]Binding energies (E_{bind}) are in kcal mol^{-1}. $\delta^{CCSDT(Q)}_{CCSD(T)} = E^{CCSDT(Q)}_{bind} - E^{CCSD(T)}_{bind}$. [b]Single-point energies are at MP2/aCVQZ-optimized geometries. [c]Single-point energies are at CCSD(T)/aTZ-optimized geometries.

canonical correlation energies obtained with the aQZ and a5Z basis sets (as well as the aTZ basis set for the SCF energy). The extrapolated binding energies reported in the Supporting Information are within 0.03 kcal mol^{-1} of the values from the explicitly correlated coupled-cluster computations. The scaling procedure associated with the SCS-MP2-F12 method provides substantial improvement over the unscaled MP2-F12 energies (Supporting Information). Nevertheless, the SCS-MP2-F12/a5Z computations still tend to overestimate the magnitude of E_{bind} (i.e., overbind), often by as much as 20 or 30% for the P_2 and PCCP dimers, respectively, relative to the CCSD(T)-F12/a5Z E_{bind} and E^{CP}_{bind} values.

CCSDT(Q) single-point energy computations have also been performed on the $(P_2)_2$ optimized structures with the aDZ and aTZ basis sets. The CCSDT(Q) binding energies can be found in Table 3 along with the differences relative to the CCSD(T) values ($\delta^{CCSDT(Q)}_{CCSD(T)} = E^{CCSDT(Q)}_{bind} - E^{CCSD(T)}_{bind}$). The analogous differences for the CCSDT binding energies ($\delta^{CCSDT(Q)}_{CCSDT} = E^{CCSDT(Q)}_{bind} - E^{CCSDT}_{bind}$) are much larger and have been relegated to the Supporting Information. With the larger aTZ basis set, CCSDT(Q) binding energies for $(P_2)_2$ are roughly 0.01 to 0.02 kcal mol^{-1} less negative than the corresponding CCSD(T) values. Patkowski and co-workers recently reported that such contributions beyond the CCSD(T) level of theory can exhibit significant basis set dependencies,[26] and the same behavior is observed here. For the CCSD(T)-optimized $(P_2)_2$ structures, the differences between the CCSD(T) and CCSDT(Q) E_{bind} values are roughly 0.01 to 0.02 kcal mol^{-1} more negative with the aDZ basis set than aTZ. This dependence raises some concerns for the larger PCCP dimer system for which the CCSDT(Q) computations were feasible only with the smaller aDZ basis set. The deviations for $(PCCP)_2$ are much larger, with magnitudes greater than 0.04 kcal mol^{-1} for several structures and exceeding 0.08 kcal mol^{-1} in one case (the MP2/aCVQZ-optimized Rec structure). If the trends observed here for $(P_2)_2$ and elsewhere for other noncovalent dimers[26] extend to $(PCCP)_2$, then the differences between the CCSD(T) and CCSDT(Q) binding energies will almost certainly exceed 0.1 kcal mol^{-1} if they are evaluated with larger basis sets (e.g., aTZ).

Given the small changes from both the CCSDT(Q) computations and the CP procedure, the CCSD(T)-F12/a5Z binding energies reported in the last column of Tables 1 and 2 are expected to be rather reliable estimates of correlated CBS limit electronic binding energies for both of these noncovalent dimer systems. The CCSD(T)-F12/a5Z computations indicate that the PS minimum of the P_2 dimer has an electronic binding energy (E_{bind}) of −1.01 kcal mol^{-1}. Applying the corresponding CCSD(T)/aTZ unscaled harmonic zero-point vibrational energy (ZPVE) correction decreases the magnitude of the binding energy to −0.93 kcal mol^{-1}. For $(PCCP)_2$, the CCSD(T)-F12/a5Z computations indicate that the three most strongly bound minima, PS, X, and T, have electronic binding energies (E_{bind}) of −2.89, −2.58, and −1.74 kcal mol^{-1}, respectively. These magnitudes are reduced when including the CCSD(T)/aTZ ZPVE corrections to −2.72, −2.46, and −1.61, respectively.

3.3.2. Interaction Energies. The interaction energies (E_{int}) have also been computed for the $(P_2)_2$ and $(PCCP)_2$ structures with a variety of methods including those based on SAPT and dispersion-corrected DFT. The complete set of data can be found in the Supporting Information, but the results are summarized in Table 4 in terms of the average and maximum absolute deviations (AvgAD and MaxAD, respectively) relative to the CCSD(T)/aTZ interaction energies. For the seven $(P_2)_2$ stationary points, the CCSD(T)/aTZ values for E_{int} range from −0.70 to −1.04 kcal mol^{-1} with an average of −0.88 kcal mol^{-1} (Supporting Information). For this small dimer, only SAPT2+3(CCD) and the two scaled CCSD techniques get within 0.1 kcal mol^{-1} (roughly 10−20%) of the reference interaction energies on average and never deviate by more than 0.2 kcal mol^{-1}. SCS-CCSD and SCS(MI)-CCSD are also the best performing wave function methods in Table 4 for $(PCCP)_2$. The average and maximum absolute deviations for these methods do not exceed 0.3 and 0.6 kcal mol^{-1}, respectively. Although the deviations for $(PCCP)_2$ are roughly a factor of 3 larger than those for $(P_2)_2$, that is entirely

DOI: 10.1021/acs.jctc.5b01105
J. Chem. Theory Comput. 2016, 12, 1534−1541

Table 4. Average and Maximum Absolute Deviations of Interaction Energies Computed with the aTZ Basis Set Relative to the CCSD(T)/aTZ E_{int} Values[a]

	P_2 dimer		PCCP dimer	
	AvgAD[b]	MaxAD	AvgAD[c]	MaxAD
MP2	0.72	0.87	1.94	2.62
MP3	0.40	0.52	1.15	1.65
MP2.5	0.16	0.23	0.39	0.56
MP2C	0.15	0.18	0.38	0.56
SCS-CCSD	0.10	0.13	0.27	0.46
SCS(MI)-CCSD	0.10	0.12	0.26	0.38
SAPT2	0.54	0.75	1.46	2.50
SAPT2+	0.14	0.38	0.48	1.06
SAPT2+3	0.13	0.35	0.39	1.01
SAPT2+3(CCD)	0.10	0.17	0.27	0.54
B97-D3BJ	0.63	0.90	0.54	0.88
B3LYP-D3BJ	0.29	0.51	0.22	0.43
ωB97X-D	0.21	0.44	0.82	0.96
APFD	0.18	0.32	0.18	0.46

[a]Average and maximum absolute deviations of interaction energies (AvgAD and MaxAD, respectively) are in kcal mol^{-1}. [b]Average for the seven CCSD(T)/aTZ-optimized geometries for $(P_2)_2$. [c]Average for the six CCSD(T)/aTZ-optimized geometries for $(PCCP)_2$.

consistent with the stronger interactions for the PCCP dimer, where E_{int} ranges from −0.95 to −2.65 kcal mol^{-1} at the CCSD(T)/aTZ level of theory with an average of −1.84 kcal mol^{-1}.

The AvgAD and MaxAD values for MP2.5 and MP2C are remarkably similar. Both methods offer significant improvement over MP2 and MP3, but they still have noticeably larger deviations than either SCS-CCSD or SCS(MI)-CCSD. MP2.5 and MP2C still overbind the X and ⊥X structures of the PCCP dimer by more than 0.5 kcal mol^{-1} (and by approximately 0.4 kcal mol^{-1} on average).

The deviations associated with the small set of dispersion-corrected DFT methods examined here vary widely. When considering both $(P_2)_2$ and $(PCCP)_2$, APFD exhibited the smallest deviations, although it was essentially tied with B3LYP-D3BJ for the PCCP dimer. In fact, the AvgAD and MaxAD values for APFD are comparable to those with the best wave function methods (SCS-CCSD and SCS(MI)-CCSD). Encouraged by these positive results, the APFD and B3LYP-D3BJ methods were used in conjunction with the aTZ basis sets to reoptimize and characterize the structures of both systems (Supporting Information). Regrettably, an L-shaped minimum was still found on the P_2 dimer surface lying a few hundredths of a kcal mol^{-1} below the PS structure. Scans about PP···PP torsional angle (Supporting Information) indicate that ωB97X-D is the only functional in the set tested for which the L-shaped stationary point does not exist. As such, the method also correctly identifies the PS structure as a minimum. Unfortunately, ωB97X-D also predicts that the npT structure is another minimum rather than a first-order saddle point according to the CCSD(T)/aTZ computations. A wider range of DFT methods will be examined in a future study.

CCSDT(Q) interaction energies were also computed with and without the counterpoise procedure. As with E_{bind}, the difference between the CCSD(T) and CCSDT(Q) values are quite small for E_{int} (Supporting Information). Although the CP procedure has a significant effect on these interaction energies, it had virtually no effect on the difference between the CCSD(T) and CCSDT(Q) data (<0.015 kcal mol^{-1}). Careful comparison of E_{bind} and E_{int} from the CCSD(T)/aTZ computations reveals that E_{int} and E_{bind} are identical to 0.001 kcal mol^{-1} for the CCSD(T)/aTZ-optimized structures of $(P_2)_2$. In the case of $(PCCP)_2$, the magnitude of E_{int} is only slightly larger than E_{bind} (by no more than 0.02 kcal mol^{-1}). Both sets of results indicate that the monomer fragments are essentially undistorted in the dimer. Consequently, the higher-order correlation effects from the CCSDT(Q) computations can actually invert the normal ordering of the two quantities so that the magnitude of E_{int} becomes slightly less than that of E_{bind}. The inconsistencies, however, can become far more pronounced for other methods and particularly for the MP2/aCVQZ-optimized structures of the dimers.

The components of E_{int} from the SAPT computations with the aTZ basis set (dispersion (E_{disp}), electrostatics (E_{elst}), induction (E_{ind}), and exchange-repulsion (E_{exch})) are provided in the Supporting Information for both the MP2/aCVQZ- and CCSD(T)/aTZ-optimized structures. Although there is a sizable decrease in all of the attractive components when the MP2/aCVQZ structures[9] are reoptimized at the CCSD(T)/aTZ level of theory (by more than 1.5 kcal mol^{-1} for $(P_2)_2$ and 4.8 kcal mol^{-1} for $(PCCP)_2$), there is a commensurate decrease in the exchange-repulsion (approaching 4 and 11 kcal mol^{-1} in $(P_2)_2$ and $(PCCP)_2$, respectively). Consequently, the overall changes to the interaction energies are only around −0.5 kcal mol^{-1} for both $(P_2)_2$ and $(PCCP)_2$. Dispersion remains the most significant attractive component to the interaction energy for these homodimers, growing to −2.1 and −5.7 kcal mol^{-1} for the PS structures of $(P_2)_2$ and $(PCCP)_2$, respectively.

For the CCSD(T)/aTZ-optimized structures, E_{disp} is the most difficult contribution to reliably describe and certainly lies at the heart of the challenges posed by these simple dimers. While the E_{exch} terms must be the same by definition for these four methods, the E_{ind} values reported in the Supporting Information are also identical to two decimal places. The values computed for E_{elst} are quite similar as well. The SAPT2, SAPT2+, and SAPT2+3 computations are usually within 0.1 kcal mol^{-1} of the SAPT2+3(CCD) E_{elst} values, and the deviations never exceed 0.27 kcal mol^{-1}. In contrast, SAPT2, SAPT2+, and SAPT2+3 always appreciably overestimate the dispersion contribution to binding, by as much as 2.32, 0.89, and 0.96 kcal mol^{-1}, respectively. Similar trends were also reported earlier for the MP2/aCVQZ-optimized structures.[9]

4. CONCLUSIONS

Seven P_2 dimer configurations and five PCCP dimer configurations have been characterized via full geometry optimizations and corresponding harmonic vibrational frequency computations with the CCSD(T) electronic structure method and the aTZ basis set. The MP2 and CCSD(T) binding energies at the CCSD(T) CBS limit for these stationary points have been determined using basis sets of up to pentuple-ζ quality. This study finds that the CCSD(T) PES can be qualitatively different from the MP2 PES. The most pronounced discrepancy occurs for $(P_2)_2$, where the L-shaped global minimum characterized on the MP2 PES does not appear to exist on the CCSD(T)/aTZ PES.

The PS structure is the only $(P_2)_2$ minimum at the CCSD(T)/aTZ level of theory with an electronic binding energy of −1.01 kcal mol^{-1} at the CCSD(T) CBS limit. In contrast, three strongly bound minima have been identified on the $(PCCP)_2$ surface. These PCCP dimer minima correspond

DOI: 10.1021/acs.jctc.5b01105
J. Chem. Theory Comput. 2016, 12, 1534−1541

to PS, X, and T configurations with CCSD(T) CBS limit binding energies of −2.89, −2.58, and −1.74 kcal mol^{-1}, respectively. The CP procedure does not appreciably change these estimated CBS limits of E_{bind} (≤0.02 kcal mol^{-1} for $(P_2)_2$ and ≤0.04 kcal mol^{-1} for $(PCCP)_2$).

CCSDT(Q) computations on the P_2 dimer system with the aDZ and aTZ basis sets yield energetics that are virtually identical to the CCSD(T) values, within 0.02 kcal mol^{-1}, when using the larger aTZ basis set. The differences between the CCSD(T) and CCSDT(Q) energetics (E_{bind} and E_{int}) are somewhat larger for the PCCP dimer, but they could be evaluated only with the smaller aDZ basis set. Given the tendency for the magnitude of these differences to increase with the size of the basis set,[26] it is likely that they will exceed 0.1 kcal mol^{-1} for certain $(PCCP)_2$ structures if a larger basis set is employed. Unfortunately, CCSDT(Q) computations on the PCCP dimer with the aTZ basis set are prohibitively demanding. We are currently working to identify relatively compact basis sets that can accurately describe the difference between CCSD(T) and CCSDT(Q) energetics to obtain a more reliable estimate of electron correlation effects beyond the CCSD(T) level of theory on the energetics of this challenging $(PCCP)_2$ system.

In stark contrast to the similarity of CCSD(T) and CCSDT(Q) energetics for these systems, the MP2.5, MP2C, SCS-CCSD, SCS(MI)-CCSD, SAPT2, SAPT2+, SAPT2+3, SAPT2+3(CCD), B97-D3BJ, B3LYP-D3BJ, ωB97X-D, and APFD interaction energies tend to deviate appreciably from CCSD(T) values obtained with the same aTZ basis set. For $(P_2)_2$, only SCS-CCSD, SCS(MI)-CCSD, and SAPT2+3(CCD) were consistently within 0.17 kcal mol^{-1} of the target E_{int} values and within 0.10 kcal mol^{-1} on average. The situation for $(PCCP)_2$ was far more grim. The best post-Hartree−Fock method, SCS(MI)-CCSD, had an AvgAD of 0.26 kcal mol^{-1} and a MaxAD of 0.38 kcal mol^{-1}. Interestingly, the APFD functional had the best AvgAD for this system (0.18 kcal mol^{-1}) and a respectable MaxAD of 0.46 kcal mol^{-1}. Unfortunately, none of the four dispersion corrected DFT methods tested here could correctly characterize the minima for both dimer systems. Nevertheless, this analysis was certainly not an exhaustive examination of modern DFT methods, and we plan to test a much wider range of functionals in the near future.

■ ASSOCIATED CONTENT

Supporting Information

The Supporting Information is available free of charge on the ACS Publications website at DOI: 10.1021/acs.jctc.5b01105.

Monomer geometrical and vibrational data, additional binding energies, interaction energies, SAPT interaction energy components, Cartesian coordinates of the CCSD(T)/aTZ optimized structures, and CCSD(T)/aTZ harmonic vibrational frequencies (PDF)

■ AUTHOR INFORMATION

Corresponding Author

*E-mail: tschumpr@olemiss.edu. Phone: +1 (662) 915-7301.

Present Address

†(E.V.D.) Department of Chemistry, Mississippi State University, Mississippi State, Mississippi 39762-9573, United States.

Funding

This work was funded in part by the National Science Foundation (EPS-0903787, CHE-1338056, and IIA-1430364).

Notes

The authors declare no competing financial interest.

■ ACKNOWLEDGMENTS

The authors acknowledge the Mississippi Center for Supercomputing Research for access to their computational resources. Prof. Ed Hohenstein (City College of New York) and Dr. Lori Burns (Georgia Institute of Technology) are thanked for their very generous assistance with some of the technical aspects of the MP2C computations.

■ REFERENCES

(1) Müller-Dethlefs, K.; Hobza, P. *Chem. Rev.* **2000**, *100*, 143−168.
(2) Černý, J.; Hobza, P. *Phys. Chem. Chem. Phys.* **2007**, *9*, 5291−5303.
(3) Riley, K. E.; Hobza, P. *WIREs Comput. Mol. Sci.* **2011**, *1*, 3−15.
(4) Martinez, C. R.; Iverson, B. L. *Chem. Sci.* **2012**, *3*, 2191−2201.
(5) Hobza, P. *Acc. Chem. Res.* **2012**, *45*, 663−672.
(6) Riley, K. E.; Hobza, P. *Acc. Chem. Res.* **2013**, *46*, 927−936.
(7) Hohenstein, E. G.; Jaeger, H. M.; Carrell, E. J.; Tschumper, G. S.; Sherrill, C. D. *J. Chem. Theory Comput.* **2011**, *7*, 2842−2851.
(8) Carrell, E. J.; Thorne, C. M.; Tschumper, G. S. *J. Chem. Phys.* **2012**, *136*, 014103.
(9) Van Dornshuld, E.; Tschumper, G. S. *J. Comput. Chem.* **2014**, *35*, 479−487.
(10) Møller, C.; Plesset, M. S. *Phys. Rev.* **1934**, *46*, 618−622.
(11) Bartlett, R. J. *Annu. Rev. Phys. Chem.* **1981**, *32*, 359−401.
(12) Purvis, G. D., III; Bartlett, R. J. *J. Chem. Phys.* **1982**, *76*, 1910−1918.
(13) Wada, A.; Kanamori, H.; Iwata, S. *J. Chem. Phys.* **1998**, *109*, 9434−9438.
(14) Leforestier, C.; Tekin, A.; Jansen, G.; Herman, M. *J. Chem. Phys.* **2011**, *135*, 234306.
(15) Hopkins, B. W.; ElSohly, A. M.; Tschumper, G. S. *Phys. Chem. Chem. Phys.* **2007**, *9*, 1550−1558.
(16) ElSohly, A. M.; Hopkins, B. W.; Copeland, K. L.; Tschumper, G. S. *Mol. Phys.* **2009**, *107*, 923−928.
(17) Copeland, K. L.; Tschumper, G. S. *J. Chem. Theory Comput.* **2012**, *8*, 4279−4284.
(18) Sinnokrot, M. O.; Valeev, E. F.; Sherrill, C. D. *J. Am. Chem. Soc.* **2002**, *124*, 10887−10893.
(19) Tschumper, G. S.; Leininger, M. L.; Hoffman, B. C.; Valeev, E. F.; Schaefer, H. F.; Quack, M. *J. Chem. Phys.* **2002**, *116*, 690−701.
(20) Hopkins, B. W.; Tschumper, G. S. *J. Phys. Chem. A* **2004**, *108*, 2941−2948.
(21) Lane, J. R. *J. Chem. Theory Comput.* **2013**, *9*, 316−323.
(22) Řezáč, J.; Šimová, L.; Hobza, P. *J. Chem. Theory Comput.* **2013**, *9*, 364−369.
(23) Řezáč, J.; Hobza, P. *J. Chem. Theory Comput.* **2013**, *9*, 2151−2155.
(24) Šimová, L.; Řezáč, J.; Hobza, P. *J. Chem. Theory Comput.* **2013**, *9*, 3420−3428.
(25) Řezáč, J.; Hobza, P. *J. Chem. Theory Comput.* **2014**, *10*, 3066−3073.
(26) Smith, D. G. A.; Jankowski, P.; Slawik, M.; Witek, H. A.; Patkowski, K. *J. Chem. Theory Comput.* **2014**, *10*, 3140−3150.
(27) Kucharski, S. a. A.; Bartlett, R. J. *J. Chem. Phys.* **1998**, *108*, 9221−9226.
(28) Kendall, R. A.; Dunning, T. H., Jr.; Harrison, R. J. *J. Chem. Phys.* **1992**, *96*, 6796−6806.
(29) Woon, D. E.; Dunning, T. H., Jr. *J. Chem. Phys.* **1993**, *98*, 1358−1371.

DOI: 10.1021/acs.jctc.5b01105
J. Chem. Theory Comput. 2016, 12, 1534−1541

(30) Stanton, J. F.; Gauss, J.; Harding, M. E.; Szalay, P. G. *CFOUR (Coupled-Cluster techniques for Computational Chemistry)*. For the current version, see http://www.cfour.de (accessed January 18, 2016).
(31) Grimme, S. *J. Chem. Phys.* **2003**, *118*, 9095−9102.
(32) Werner, H.-J.; Knowles, P. J.; Knizia, G.; Manby, F. R.; Schütz, M.; Celani, P.; Györffy, W.; Kats, D.; Korona, T.; Lindh, R.; Mitrushenkov, A.; Rauhut, G.; Shamasundar, K. R.; Adler, T. B.; Amos, R. D.; Bernhardsson, A.; Berning, A.; Cooper, D. L.; Deegan, M. J. O.; Dobbyn, A. J.; Eckert, F.; Goll, E.; Hampel, C.; Hesselmann, A.; Hetzer, G.; Hrenar, T.; Jansen, G.; Köppl, C.; Liu, Y.; Lloyd, A. W.; Mata, R. A.; May, A. J.; McNicholas, S. J.; Meyer, W.; Mura, M. E.; Nicklass, A.; O'Neill, D. P.; Palmieri, P.; Peng, D.; Pflüger, K.; Pitzer, R.; Reiher, M.; Shiozaki, T.; Stoll, H.; Stone, A. J.; Tarroni, R.; Thorsteinsson, T.; Wang, M. *MOLPRO, a Package of Ab Initio Programs*, version 2010.1; 2010. http://www.molpro.net (accessed January 18, 2016).
(33) Liu, B.; McLean, A. D. *J. Chem. Phys.* **1973**, *59*, 4557−4558.
(34) Jansen, H. B.; Ros, P. *Chem. Phys. Lett.* **1969**, *3*, 140−143.
(35) Boys, S.; Bernardi, F. *Mol. Phys.* **1970**, *19*, 553−566.
(36) Tschumper, G. S. In *Reviews in Computational Chemistry*; Lipkowitz, K. B., Cundari, T. R., Eds.; John Wiley & Sons, Inc.: Hoboken, NJ, 2009; Vol. *26*; pp 39−90.
(37) Hohenstein, E. G.; Sherrill, C. D. *J. Chem. Phys.* **2010**, *133*, 014101.
(38) Turney, J. M.; Simmonett, A. C.; Parrish, R. M.; Hohenstein, E. G.; Evangelista, F. A.; Fermann, J. T.; Mintz, B. J.; Burns, L. A.; Wilke, J. J.; Abrams, M. L.; Russ, N. J.; Leininger, M. L.; Janssen, C. L.; Seidl, E. T.; Allen, W. D.; Schaefer, H. F.; King, R. A.; Valeev, E. F.; Sherrill, C. D.; Crawford, T. D. *Wiley Interdisciplinary Reviews: Computational Molecular Science* **2012**, *2*, 556−565.
(39) Grimme, S. *J. Comput. Chem.* **2006**, *27*, 1787−1799.
(40) Grimme, S.; Ehrlich, S.; Goerigk, L. *J. Comput. Chem.* **2011**, *32*, 1456−1465.
(41) Becke, A. D. *J. Chem. Phys.* **1993**, *98*, 5648−5652.
(42) Lee, C.; Yang, W.; Parr, R. G. *Phys. Rev. B: Condens. Matter Mater. Phys.* **1988**, *37*, 785−789.
(43) Chai, J.-D.; Head-Gordon, M. *Phys. Chem. Chem. Phys.* **2008**, *10*, 6615−6620.
(44) Austin, A.; Petersson, G. A.; Frisch, M. J.; Dobek, F. J.; Scalmani, G.; Throssell, K. *J. Chem. Theory Comput.* **2012**, *8*, 4989−5007.
(45) Frisch, M. J.; Trucks, G. W.; Schlegel, H. B.; Scuseria, G. E.; Robb, M. A.; Cheeseman, J. R.; Scalmani, G.; Barone, V.; Mennucci, B.; Petersson, G. A.; Nakatsuji, H.; Caricato, M.; Li, X.; Hratchian, H. P.; Izmaylov, A. F.; Bloino, J.; Zheng, G.; Sonnenberg, J. L.; Hada, M.; Ehara, M.; Toyota, K.; Fukuda, R.; Hasegawa, J.; Ishida, M.; Nakajima, T.; Honda, Y.; Kitao, O.; Nakai, H.; Vreven, T.; Montgomery, J. A., Jr.; Peralta, J. E.; Ogliaro, F.; Bearpark, M.; Heyd, J. J.; Brothers, E.; Kudin, K. N.; Staroverov, V. N.; Kobayashi, R.; Normand, J.; Raghavachari, K.; Rendell, A.; Burant, J. C.; Iyengar, S. S.; Tomasi, J.; Cossi, M.; Rega, N.; Millam, J. M.; Klene, M.; Knox, J. E.; Cross, J. B.; Bakken, V.; Adamo, C.; Jaramillo, J.; Gomperts, R.; Stratmann, R. E.; Yazyev, O.; Austin, A. J.; Cammi, R.; Pomelli, C.; Ochterski, J. W.; Martin, R. L.; Morokuma, K.; Zakrzewski, V. G.; Voth, G. A.; Salvador, P.; Dannenberg, J. J.; Dapprich, S.; Daniels, A. D.; Farkas, O.; Foresman, J. B.; Ortiz, J. V.; Cioslowski, J.; Fox, D. J. *Gaussian 09*, revision B.01; Gaussian, Inc.: Wallingford, CT, 2009.
(46) Takatani, T.; Hohenstein, E. G.; Sherrill, C. D. *J. Chem. Phys.* **2008**, *128*, 124111.
(47) Pitoňák, M.; Řezáč, J.; Hobza, P. *Phys. Chem. Chem. Phys.* **2010**, *12*, 9611−9614.
(48) Pople, J. A.; Binkley, J. S.; Seeger, R. *Int. J. Quantum Chem.* **1976**, *10*, 1−19.
(49) Pople, J. A.; Seeger, R.; Krishnan, R. *Int. J. Quantum Chem.* **1977**, *12*, 149−163.
(50) Pitoňák, M.; Neogrády, P.; Černý, J.; Grimme, S.; Hobza, P. *ChemPhysChem* **2009**, *10*, 282−289.
(51) Heßelmann, A. *J. Chem. Phys.* **2008**, *128*, 144112.
(52) Pitoňák, M.; Heßelmann, A. *J. Chem. Theory Comput.* **2010**, *6*, 168−178.

DOI: 10.1021/acs.jctc.5b01105
J. Chem. Theory Comput. 2016, 12, 1534−1541